Journal of Membrane Science 669 (2023) 121331

Contents lists available at ScienceDirect

Journal of Membrane Science

journal homepage: www.elsevier.com/locate/memsci

Polyisatin derived ion-solvating blend membranes for alkaline water electrolysis

M. Makrygianni [a], S. Aivali [a], Y. Xia [b], M.R. Kraglund [b], D. Aili [b,**], V. Deimede [a,*]

[a] Department of Chemistry, University of Patras, GR 26504, Patras, Greece
[b] Department of Energy Conversion and Storage, Technical University of Denmark, Fysikvej, Building 310, 2800 Kgs, Lyngby, Denmark

ARTICLE INFO

Keywords:
Ion-solvating polymers
Alkaline membrane
poly(ethylene oxide)
Isatin
Alkaline water electrolysis

ABSTRACT

It is a great challenge to develop membranes based on polyaromatic backbone chemistries that combine high alkaline resistance with high ionic conductivity and low gas crossover for alkaline water electrolysis. Hence, a new alkaline stable aromatic monomer containing side ion-solvating poly(ethylene oxide) (PEO) groups was synthesized and polymerized with isatin and biphenyl via super acid catalyzed hydroxyalkylation to yield ion-solvating copolymers. The prepared aryl-ether free backbone aromatic copolymers (P(IB-PEO)-y) have excellent film-forming properties, high thermal stability, but moderate KOH electrolyte uptake and relatively low conductivity. Therefore, to further enhance the electrolyte uptake and ionic conductivity, P(IB-PEO)-20 copolymers were blended with polybenzimidazole in ratios 80/20, 70/30, 60/40 and 50/50. The prepared blend membranes exhibit high electrolyte uptakes (up to 97 wt%) while the highest ionic conductivity of 110 mS cm^{-1} at 80 °C was observed for PBI80/P(IB-PEO) blend. The KOH doped PBI70/P(IB-PEO) membrane shows a tensile strength of 20 MPa and a significant increase in Young's modulus (131%) compared to that of PBI80/P(IB-PEO). The alkaline stability test demonstrated that PBI80/P(IB-PEO) membrane exhibits a substantially higher Young's modulus (144% increase) than non-aged analogue, after 1 month in 20 wt% KOH solution at 80 °C. Further, PBI80/P(IB-PEO) and PBI70/P(IB-PEO) membranes retained 96–98% of their original conductivity after aging, indicating their excellent alkaline resistance. Selected membranes were tested in a single cell electrolyzer to probe feasibility and crossover behaviour.

1. Introduction

Water electrolysis is a key technology enabling the production of hydrogen and oxygen via electrochemical splitting of water [1]. Hydrogen has been long recognized as a promising alternative energy carrier to replace fossil fuels for power generation in transportation, industrial sector and residential heating [2–4]. When hydrogen is generated using renewable energy, it has the potential to be a zero-carbon energy carrier, thus facilitating the green transition to a more secure, sustainable energy system [5,6]. There are two commercial water electrolysis technologies at low temperatures, the conventional alkaline electrolyzers that use highly concentrated aqueous KOH solution as electrolyte and a porous separator and the proton exchange membrane (PEM) electrolyzers. Although abundant and inexpensive platinum-free catalysts can be utilized under alkaline conditions, alkaline electrolyzers suffer from high internal resistance and product gas crossover through the porous separator. This has driven to the replacement of the porous separator with a non-porous, dense polymeric membrane, a proton exchange membrane system (PEM) that offers several advantages including high-purity hydrogen production and high current densities with a theoretical efficiency of 80–90%. Nevertheless, PEM electrolyzers are expensive and depend on precious platinium group electrocatalysts such as platinium for the cathode and iridium for the anode. In addition, large scale system implementation is practically unfeasible due to the limited availability of iridium which is much rarer that platinum [7,8].

Anion exchange membranes (AEM) water electrolyzers have gained much attention the last decade as an alternative solution that addresses the drawbacks and combines the merits of PEM and conventional alkaline water electrolyzers [7–13]. However, the insufficient OH^- ion conductivity and mainly the lack of chemical stability of AEMs are critical factors that hinder their practical use [14]. Regarding the

* Corresponding author.
** Corresponding author.
E-mail addresses: larda@dtu.dk (D. Aili), deimede@upatras.gr (V. Deimede).

https://doi.org/10.1016/j.memsci.2022.121331
Received 6 April 2022; Received in revised form 20 October 2022; Accepted 26 December 2022
Available online 27 December 2022

chemical stability, both cationic moieties and polymer backbone in AEMs are susceptible to nucleophilic attack by hydroxide ions, leading to the loss of conductivity and mechanical strength, which in turn causes a failure in alkaline electrolyzers. Therefore, several approaches have been proposed to ameliorate the degradation of functional cationic groups in alkaline media but so far, although much progress has been made the durability of AEMs remains a big challenge [15].

Redesigning the AEM electrolyzers towards improved chemical stability and cell performance is a strategy to circumvent the limitations of AEM technology. To succeed this, a recently suggested strategy is the ion-solvating membrane concept [16–18]. In this concept, a dense polymeric membrane in combination with a supporting aqueous alkaline electrolyte (KOH solution) is required to achieve the good cell performance, since the conductive properties are associated with membrane's ability to be doped in KOH solution and the presence of the respective electrolyte. Typical ion-solvating membranes are based on poly(ethylene oxide) (PEO) [19], poly(vinyl alcohol) (PVA) [20,21] and polybenzimidazole (PBI) [22,23]. The most well investigated system is the KOH (aq) doped poly(2,2'-(*m*-phenylene)-5,5′-bibenzimidazole) (*m*-PBI), which has demonstrated impressive cell performance [16]. However, very recently, PBI-based ion-solvating membranes such as poly [2,2'-(1,4-naphthalene)-5,5′-bibenzimidazole] (NPBI) and its sulfonated functionalized analogues were explored as promising alternatives for alkaline water electrolysis application [24,25]. In particular, sulfonate grafted NPBI in which sulfonate side chains are attached to PBI backbone shows improved KOH electrolyte uptake and consequently higher ionic conductivity along with improved cell performance when compared with the unmodified NPBI membrane [24].

The lack of cationic groups which are vulnerable to degradation by hydroxide attack consists a major benefit of ion-solvating polymers. Thus, the chemical stability of the polymer backbone in ion-solvating polymers should be the only critical concern to be solved and consequently the focus should be shifted towards alkaline stable backbone chemistries with high electrolyte uptake.

For polymeric backbones, the presence of heteroatoms and electron-withdrawing groups in the polymer backbone, particularly the polymers containing arylene ether and sulfone linkages, is correlated with poor alkaline stability [26]. Therefore, the search for alkaline stable backbones is directed towards polyaromatic backbone chemistries [27]. Among these synthetic methods of preparing aryl ether-free polyaromatics, superacid-catalyzed polyhydroxyalkylation has become an easy synthetic route to get linear aromatic polymers with high molecular weights polymers and high reaction efficiency [28–30]. Very recently, aryl ether free polyaromatics were synthesized via super-acid catalyzed polymerization and exhibited excellent chemical stability under alkaline media [31–40].

As such, the idea was to design and synthesize aryl-ether free aromatic backbone copolymers containing ion-solvating side PEO and isatin segments. These polymeric structures combine very attractive properties. In specific, the presence of both isatin and ion-solvating PEO segments bearing polar ether groups which can solvate the K^+ cations via acid-donor interactions promotes the high electrolyte uptake while the poly aromatic backbone, free of alkaline labile aryl ether linkages can ensure the high alkaline stability and the mechanical robustness. In addition, the excellent alkaline stability of isatin based copolymers owing to the steric effect of bulky adjacent phenyl ring to C2-carbon, is already reported by several groups [33,36,40].

Herein, a new series of aryl-ether free main backbone copolymers containing ion-solvating side PEO and isatin groups (P(IB-PEO)-y) were prepared via superacid-catalyzed polyhydroxyalkylation of biphenyl, isatin and PEO side functionalized *p*-terphenyl. To the best of our knowledge, is the first attempt to use this synthetic route for preparing ion-solvating polymers bearing two different groups that can interact with KOH solution. High molecular weight ion-solvating polymers were obtained and mechanically stable membranes were fabricated. In order to tune the membrane properties and further promote electrolyte uptake, the polymers where blended with *m*-PBI at different ratios [41]. The membranes were systematically characterized with respect to physicochemical properties and alkaline stability and evaluated in alkaline electrolyzer tests.

2. Experimental

2.1. Materials

m-PBI powder and membranes were supplied by Blue Word Technologies. Poly(ethylene oxide) methyl ether tosylate, 2,5-dibromohydroquinone and 2,5-dibromo-1,4-bis(methoxy poly(ethylene oxide)) benzene were synthesized according to a known procedure [42,43]. Benzeneboronic acid (98%, Alfa Aesar), bis(triphenylphosphine)palladium (II) dichloride (99.99%, Sigma Aldrich), potassium carbonate (K_2CO_3, 99%), biphenyl (99%, Alfa Aesar), *p*-toluenesulfonyl chloride (TsCl, 98%, Sigma-Aldrich), isatin (98%, Alfa Aesar), trifluoracetic acid (TFA, 99%, Alfa Aesar), trifluoromethanesulfonic acid (TFSA, 99%, Fluorochem), potassium hydroxide (+85% pellets, Merck), *N*,*N*-dimethylacetamide (DMA, 99.5%, Scharlab), toluene (Scharlab), ethyl acetate (Sigma Aldrich), methanol (Sigma Aldrich), dichloromethane (Scharlab), *N*,*N*-dimethylformamide-d_7 (99.50 atom% Deutero DE), chloroform-*d* (99.80 atom% Deutero DE) were all used as received. Ni foam (pore size 450 μm, thickness 1.6 mm) was obtained from Alantum.

2.2. Synthesis of PEO side functionalized p-terphenyl monomer

The PEO side functionalized *p*-terphenyl monomer was synthesized in three steps, as shown in Scheme 1. The two first steps involving the tosylation of poly(ethylene glycol) methyl ether followed by reaction with 2,5-dibromo-benzene-1,4-diol, have already been described by our group [42,43]. In the last step, the product 2,5-dibromo-1,4-bis(methoxypoly(ethylene oxide)) benzene reacted with phenylboronic acid via Suzuki coupling to give the desired monomer. The detailed synthesis is as follows. 2,5-Dibromo-1,4-bis(methoxy poly(ethylene oxide)) benzene (7.67 g, 8.24 mmol, 1 eq), benzeneboronic acid (3.01 g, 24.7 mmol, 3 eq), $PdCl_2(PPh_3)_2$ (0.30 g 0.41 mmol, 0.05 eq), aqueous solution of 2 M K_2CO_3 (20.6 mL) and toluene (42 mL) were added in a dry degassed flask. The reaction mixture was heated under reflux for 24 h. After cooling at room temperature, the water phase was separated from the organic one. The water phase was extracted with toluene and the combined organic phases were washed with water and brine, subsequently dried over $MgSO_4$ and concentrated under vacuum. The obtained light brown oily product was further purified by using column chromatography (toluene/ethyl acetate 1:1) and isolated in 76% yield.

2.3. Synthesis of P(IB-PEO)-y copolymers

The synthesis of aromatic copolymers bearing isatin and PEO side functionalities was carried out via superacid-catalyzed step-growth polymerization. A typical example of polymer preparation is as follows. Isatin (0.44 g, 2.97 mmol), biphenyl (0.33 g, 2.16 mmol), *p*-terphenyl-PEO (0.5 g, 0.54 mmol) and TFA (3.3 mL) were added into a dry degassed flask, cooled to 0–5 °C using an ice bath and stirred for 0.5 h. Subsequently, 3.8 mL of TFSA was slowly added into the mixture that was left at room temperature under vigorous stirring for 4 h until a highly viscous dark-green solution was obtained. Then, it was precipitated into methanol and an orange fibrous polymer was formed. The polymer was filtered off, washed with hot methanol and finally was dried overnight in vacuum oven at 80 °C and isolated in 86–93% yield. The synthesized copolymers are hereafter referred to as P(IB-PEO)-y, where y denotes the molar percentage of PEO side functionalized *p*-terphenyl monomer and IB abbreviation corresponds to biphenyl-isatin segment.

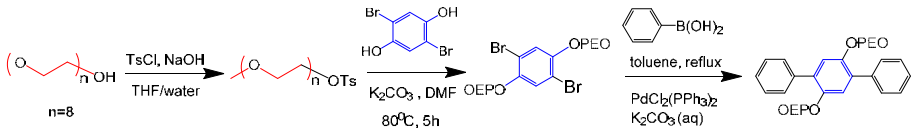

Scheme 1. Synthesis of PEO side functionalized *p*-terphenyl monomer.

2.4. Blend membrane preparation

The two blend components, P(IB-PEO)-20 and *m*-PBI were separately dissolved in DMA to obtain 5 wt% solutions, respectively. The two solutions were mixed together under stirring and the combined solution was filtered through filter paper and cast onto a clean glass plate in an oven at 80 °C for 24 h. The formed membranes were peeled off from the glass plate and dried in a vacuum oven at 100 °C for at least 20 h. Membranes with different compositions were prepared by adjusting the weight ratio of the two blend components (see Table 1). The thickness of the fabricated membranes was 50 μm and 100 μm respectively.

2.5. Characterization

The proton Nuclear Magnetic Resonance (^{1}H NMR) spectra were recorded on an Advance DPX 400 MHz spectrometer (Bruker). The samples were dissolved in DMF-d_7 or $CDCl_3$ and the chemical shifts are reported relative to tetramethylsilane (TMS) which was used as internal standard. The intrinsic viscosity of P(IB-PEO) copolymers was determined at 25 °C using an Ostwald viscometer with the copolymers dissolved in DMA. The efflux time was measured three times at four or five different concentrations of each sample. The reduced and inherent viscosities were calculated according to the following equations:

$$\eta_{inh} = \frac{\ln\left(\frac{t_1}{t_2}\right)}{c} \quad (1)$$

$$\eta_{red} = \frac{\frac{t_1}{t_2} - 1}{c} \quad (2)$$

Where t_1 is the efflux time for the polymer solution with concentration c and t_2 is the efflux time for the blank sample. The intrinsic viscosity was determined by extrapolating both η_{inh} and η_{red} to zero concentration and calculating the average intersection with the y-axis.

Thermogravimetric analysis (TGA, Labsys TG, Setaram Instrumentation) was performed in the temperature range from room temperature to 800 °C under nitrogen atmosphere and a heating rate of 20 °C min^{-1}. Attenuated Total Reflection Fourier Transform Infra-Red (ATR-FTIR) spectra were recorded on a Platinum ATR spectrometer (Bruker). The cross-surface imaging was carried out using a LEO Supra 35VP scanning electron microscope (Zeiss). The specimens were prepared by fracturing the membranes in liquid nitrogen. Mechanical properties including tensile strength, elongation at break and Young's modulus were measured using a Precision Universal/Tensile Tester (Autograph AGS-X, Shimadzu) at a cross speed of 10 min/min at room temperature. At least five identical samples were measured for each membrane and the average value was selected.

Contact angle measurements were recorded using the sessile drop method on a Kruss drop shape analyzer (DSA25). Dry membrane samples were fixed on the stage and wiped with lint free cloth, after which a 2 μl water drop was deposited. The drop was left to settle for 10 s before sampling.

Table 1
Blend composition.

Membrane Name	Blend ratio *m*-PBI: P(IB-PEO)-20	*m*-PBI(wt %)	P(IB-PEO)-20 (wt %)
PBI80/P(IB-PEO)	80/20	80	20
PBI70/P(IB-PEO)	70/30	70	30
PBI60/P(IB-PEO)	60/40	60	40
PBI50/P(IB-PEO)	50/50	50	50

2.6. Electrolyte uptake and swelling ratio

Membranes were dried under vacuum at 80 °C for 24 h before electrolyte uptake and swelling measurements. The dried membranes were immersed in 20 wt% aqueous KOH solution for 15 h at 80 °C. The electrolyte uptake, which is the difference in the weights before (m_{dry}) and after soaking the membranes in electrolyte solution (m_{wet}), was calculated according to Equation (3).

$$Electrolyte\ uptake = \frac{m_{wet} - m_{dry}}{m_{dry}} \times 100\% \quad (3)$$

The swelling ratios SR_a and SR_t were determined based on the measured area (a) and thickness (t) before (dry dimensions) and after immersion (wet dimensions) in 20 wt% aqueous KOH solution for 15 h at 80 °C. The swelling ratios were then calculated according to Equations (4) and (5), where a_{wet} and a_{dry} are the areas (length x width) of the wet and dry membranes, and t_{wet}, t_{dry} are the thicknesses of the wet and dry membranes, respectively.

$$SR_a = \frac{a_{wet} - a_{dry}}{a_{dry}} \times 100\% \quad (4)$$

$$SR_t = \frac{t_{wet} - t_{dry}}{t_{dry}} \times 100\% \quad (5)$$

2.7. Ionic conductivity

The through plane ionic conductivity of the membranes was measured at 20, 40, 60, 80 °C by ac impedance spectroscopy. The measurements were carried out using a home-made Teflon cell on AUTOLAB electrochemical workstation (PGSTAT 302 N) equipped with a frequency response analyzer ranging from 10 Hz to 1000 kHz. The membranes were sandwiched between two perforated plate nickel electrodes of active area 4 cm^2 and the cell was filled with 20 wt% aqueous KOH solution. Before conductivity measurements, the samples were equilibrated in the respective doping solution at 80 °C for 15 h. The ionic conductivity was calculated according to Equation (6), where l is the thickness of the membrane, A is the active area of the electrodes and R is the ohmic resistance between the electrodes (taken as the intercept with the real axis of the Nyquist plot).

$$\sigma = \frac{l}{A \times R} \quad (6)$$

For each membrane, two samples were prepared and measured and the average value of the two measurements was reported.

2.8. Alkaline stability

The alkaline stability of the membranes was evaluated in 20 wt% aqueous KOH solution at 80 °C. Sampling was done at pre-determined intervals and the changes in mechanical properties, hydroxide conductivity were recorded and the structural variation before and after alkaline stability test were also analyzed by ATR-FTIR and TGA.

2.9. Electrolyser testing

Alkaline electrolysis test was carried out by die-cutting membrane and Ni foam to circular specimens with a diameter of 56 mm for membrane, and 36 mm for electrodes (10 cm^2). The membrane was doped in electrolyte overnight before test, and Ni foam electrodes were pressed to a thickness of 300 μm. Membrane and electrodes were assembled with PTFE gaskets chosen to match the assembly, in a lab scale single cell electrolyser. Heating was done directly in the flowfield plate, and 20 wt% KOH electrolyte was circulated at 80 mL min^{-1} in a partially separated mode. Following an initial break-in at 100 mA cm^{-2} for 1 h at 40 °C, sequential measurements were carried out at 40, 60 and 80 °C. First impedance spectroscopy was recorded for all temperatures at both 10 and 100 mA cm^{-2} in the range 10^5 to 10^{-1} Hz using an RMS amplitude of 5–10% of the applied current density. Thereafter crossover was probed by applying a constant current density for 6 h segments, at 50, 100, 150, 200 and 400 mA cm^{-2}, followed by a polarization curve. This was repeated for all temperatures, starting at 40 °C, after which EIS measurements were repeated. Lastly the experiment was continued for one day at 40 °C and 100 mA cm^{-2}. Power was supplied by an Elektro Automatik PS 5040 40 A power supply, and system control, as well as heating and data logging was managed by a LabView interface. Impedance spectroscopy was recorded using a VersaStat 3 potentiostat (Princeton Applied Research). Impedance fitting was done using RavDav [Graves, C. RAVDAV data analysis software, version 0.9.7, 2012].

Hydrogen in oxygen levels was measured in the oxygen stream after passing through a drying column containing indicating silica gel. The hydrogen sensor was a direct electrochemical H_2 sensor, 0–40.000 ppm supplied by Geopal Systems. Recorded values were linearly scaled on basis of calibration measurements with a 1000 ppm H_2 in N_2 reference gas, carried out after the cell test experiment.

The electrolyte degassing vessels were continuously flushed with nitrogen (16 mL min^{-1}) to reduce gas sensor latency and improve signal consistency. Presented H_2 levels, X_{H2}, have been corrected for the nitrogen gas fraction unless otherwise stated. The hydrogen crossover flux φ_{H2} was calculated according to Equation (7), where N_{O2} is the oxygen production rate calculated from the applied current, and N_{N2} the nitrogen flushing rate, assuming a negligible loss of O_2 and N_2 due to crossover.

$$\varphi_{H2} = \frac{N_{O2} + N_{N2}}{\frac{1}{X_{H2,meas}} - 1} \tag{7}$$

The final relative hydrogen in oxygen gas fraction is found from the flux density by Equation (8).

$$X_{H2,cor} = \frac{\varphi_{H2}}{N_{O2} + \varphi_{H2}} \tag{8}$$

3. Results and discussion

3.1. Monomer, polymer synthesis and characterization

The super acid catalyzed hydroxyalkylation became recently a very attractive route to yield ether-free aromatic polymers combining the thermal stability with the mechanical robustness and the alkali resistance [31–33]. The synthesis and study of polyaromatics containing isatin segments for use as AEMs following this route was reported very recently, suggesting the excellent chemical stability of isatin segments under both *ex situ* and *in situ* electrolyzer durability testing [33,36,40]. Inspired by these works, a series of new copolymers was synthesized via the facile super acid catalyzed hydroxyalkylation using biphenyl, isatin and PEO side functionalized *p*-terphenyl as comonomers to study the feasibility of the ion-solvating concept. Isatin was selected due to the presence of N–H group, which can be deprotonated under alkaline conditions, to promote water and KOH uptake. The PEO side functionalized *p*-terphenyl was chosen as it combines the mechanical robustness of the terphenyl moiety with the ion-solvating properties of PEO side functionalities. This monomer was synthesized in three steps as shown in Scheme 1. The monomer synthesis started with tosylation of poly (ethylene glycol) methyl ether followed by reaction of tosylate product with 2,5-dibromo-benzene-1,4-diol, as already reported in the literature [42,43]. In the last step, reaction with phenylboronic acid via Suzuki coupling yields in the desired monomer. The structural identity and the purity of the synthesized monomer was confirmed by ^{1}H NMR spectroscopy (Fig. 1a). The signals from the aromatic protons appeared as three multiplets between 7.30 and 7.60 ppm and as a singlet located at 7.00 ppm. The strong signal in the 3.54–3.63 ppm region corresponds to the methylene protons of the ethylene oxide repeating units, while the peaks at 4.10 and 3.73 ppm are attributed to the methylene protons in α and β position to the oxygen of the C–O bond, respectively [43].

PEO side functionalized *p*-terphenyl monomer was used as a model compound to probe the stability of the PEO side functionalities due to their contribution on KOH uptake. The stability was evaluated by immersing the monomer in 20 wt% KOH solution at 80 °C for 1 month. As depicted in Fig. 1b, no new signals were appeared in the ^{1}H NMR spectrum, indicating the excellent alkaline stability of PEO groups.

The polycondensation type reaction between isatin (ketone) and electron-rich phenyl monomers took place at room temperature using a superacidic reaction mixture of TFSA/TFA to produce high molecular weight copolymers containing exclusively aromatic and isatin groups in the stiff backbone structure and side ion-solvating PEO functionalities (Scheme 2). Protonation of ketone group of isatin by TFSA leads to the formation of a super electrophilic compound, which then rapidly reacts, with the aromatic monomers. The polymerization was performed using a 10% molar excess of isatin to increase both the polymerization rate and degree of polymerization, as the presence of a small excess of carbonyl monomer greatly improves the polycondensation efficiency [44].

Tuning the feed ratio between biphenyl and PEO side functionalized *p*-terphenyl yielded in a series of copolymers with different molar

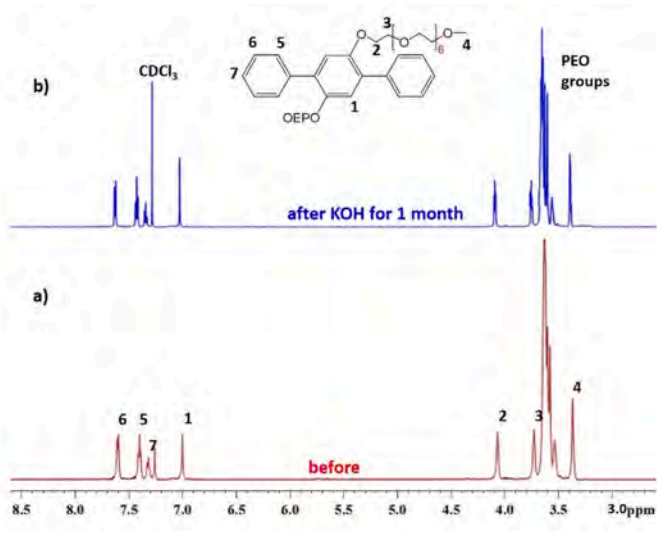

Fig. 1. ^{1}H NMR spectrum of PEO side functionalized *p*-terphenyl monomer a) before and b) after alkaline treatment with 20 wt% KOH solution at 80 °C for 1 month.

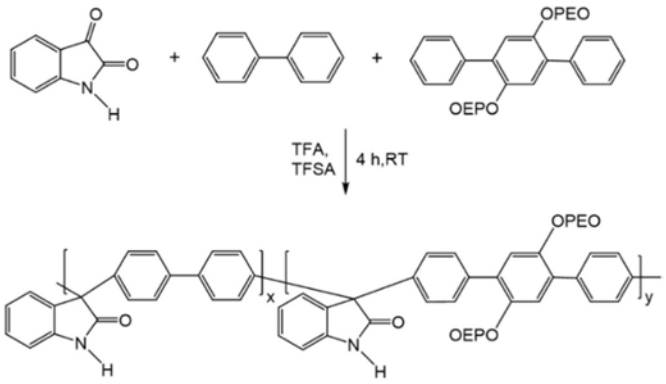

Scheme 2. Synthesis of P(IB-PEO)-y copolymers.

percentages of ion-solvating PEO groups (Table 2). To balance the conductivity and the solubility of P(IB-PEO)-y copolymers, *y* was controlled between 20 and 30%. When *y* was 100%, the resulting homopolymer was a sticky solid without film-forming ability. Solubility tests showed that the obtained copolymers were insoluble in common organic solvents, such as chloroform, tetrahydrofuran, but are soluble in dimethylsulfoxide (DMSO), *N*-methyl-2-pyrrolidone (NMP), *N*,*N*-dimethylacetamide (DMA) and *N*,*N*-dimethylformamide (DMF). Therefore, due to their insolubility in $CHCl_3$, GPC analysis could not be performed to estimate the molecular weights. The intrinsic viscosity [η] of P(IB-PEO)-30 and P(IB-PEO)-20 in DMA was calculated to be 0.58 and 0.69 dL g^{-1}, respectively (Table 2). These values are also comparable with other aryl-ether free polyaromatics bearing isatin groups prepared by superacid-catalyzed polymerization [33,34]. Although P(IB-PEO)-20 copolymers with higher intrinsic viscosity values (i.e. 0.95–1.09 dL g^{-1}) were also obtained, their partial solubility in DMA was a limiting factor for the preparation of membranes.

The molecular structure of the prepared copolymers was confirmed by ^{1}H NMR spectroscopy. The ^{1}H NMR spectrum of copolymer P(IB-PEO)-20 (DMF-d_7 was used as a solvent) is illustrated in Fig. 2. The signal at 10.8 ppm is attributed to the N–H proton of isatin [33,36]. A set of signals were observed between 7.10 ppm and 7.75 ppm, which were ascribed to the protons of terphenyl, biphenyl rings and isatin phenyl signals. The central peak at 3.43 ppm corresponds to the methylene groups of the ethylene oxide repeating unit while the signals at 4.20 and 3.73 ppm are assigned to the protons of methylene groups in α and β position to the oxygen of the C–O bond. The peak at 3.23 ppm (peak **13**) is ascribed to the to the terminal –OCH_3 groups of the PEO chain [43]. The actual composition of the synthesized copolymers and thus the molar ratio of PEO functional groups in the P(IB-PEO)-y copolymers was calculated by comparing the integral area of N–H peak with the PEO protons (peaks **1** and **11** respectively). As shown in Table 2, the molar ratio of PEO functional groups calculated from the ^{1}H NMR data agrees very well with the feed ratio, suggesting the high reactivity of monomers.

The structural identity of the synthesized copolymers was further supported by ATR-FTIR spectroscopy (Fig. S1). The broad peak located at 3485 cm^{-1} is assigned to the N–H stretching of isatin in P(IB-PEO)-20 while the characteristic band at 1710 cm^{-1} corresponds to the C═O stretching of the amide bond [36]. In addition, the peaks at 1619, 1484 cm^{-1} and 2868 cm^{-1} are assigned to the C═C stretching of benzene ring and the stretching vibration of methylene groups of PEO side chains, respectively.

The thermal stability of the prepared copolymers was investigated by TGA. As shown in Table 2 and Fig. S2, all copolymers showed a two-step weight loss. The first onset of degradation at around 330 °C is attributed to the loss of PEO side groups, which is in line with other PEO based polymers [43]. The second degradation step begins at 420 °C and corresponds to the polymer backbone decomposition, which is consistent with other reported ether-free polyaromatics based AEMs [33,36]. In conclusion, these copolymers display excellent thermal stability and consequently can meet the requirement for alkaline electrolyzer applications.

Due to their high molecular weights, transparent, mechanical robust and flexible membranes were prepared by solution casting from 5 wt% solution in DMA. The resulting membranes are depicted in Fig. 3.

Having in mind that electrolyte uptake plays a key role in achieving high ionic conductivity, the electrolyte uptake for the prepared copolymers is reported in Table 2. The pristine copolymers exhibited moderate electrolyte uptake values up to 45 wt%. It was anticipated that since PEO has ion-solvating properties, the copolymer with the higher PEO molar content should possess higher electrolyte uptake. Surprisingly, the opposite behaviour was observed, which could be ascribed to the formation of a more compact structure in the case of copolymer with 30% PEO molar content, which impedes electrolyte uptake. In particular, intermolecular interactions increase with increasing PEO content due to participation of polar ether groups in strong interchain forces, thus resulting in a more compact structure with decreased free volume and consequently limited electrolyte uptake ability. The conductivity of the prepared membranes was studied at room temperature (Table 2). The prepared copolymers exhibit relatively low hydroxide conductivity values in the range of 0.1–0.8 mS cm^{-1}.

3.2. Blend membrane preparation and characterization

To further promote electrolyte uptake and to reach technologically relevant conductivities for electrolysis applications, the respective P(IB-PEO)-20 copolymer was blended with *m*-PBI, which can be sufficiently doped with KOH solution to ensure high hydroxide conductivity. The resulting blend membranes (PBI/P(IB-PEO)) containing 80, 70 and 60 wt% *m*-PBI content were transparent and flexible, as depicted in Fig. S3. Moreover, all blend membranes present a homogeneous structure, as revealed by SEM (Fig. S4).

3.2.1. Electrolyte uptake, swelling ratio and contact angle

Both *m*-PBI and copolymer bearing isatin and PEO groups can absorb water and KOH via acid-base and hydrogen bonding interactions, undergoing dimensional changes during doping with aqueous KOH solution (20 wt%). In Fig. 4a, the electrolyte uptake of blend membranes is plotted against the *m*-PBI content in the blends. It is evident that electrolyte uptake is increased with increasing *m*-PBI weight content in blends. For instance, the blend with 80 wt% *m*-PBI content displayed an electrolyte uptake of 97%, which was lower compared to that of pure *m*-PBI (124%) but higher than that of the pure P(IB-PEO)-20 copolymer (42%). It shows that the electrolyte uptake could be carefully tuned by adjusting the ratio between the individual polymers with intrinsically different affinity for the aqueous electrolyte. Similar KOH uptake data

Table 2
Molecular characteristics and physical properties of P(IB-PEO)-y copolymers.

Polymer	Composition x/y (mol%)	^{1}H NMR composition x/y (mol%)	[η]dL g^{-1}[b]	$T_{d,5\%}$ (°C)	Electrolyte uptake (%)	σ(mS cm^{-1})[a]
P(IB-PEO)-20	80/20	80/20	0.69	368	45	0.8
P(IB-PEO)-30	70/30	72/28	0.58	351	31	0.1

[a] Measured in 20 wt% KOH at room temperature.
[b] In DMA at 30 °C.

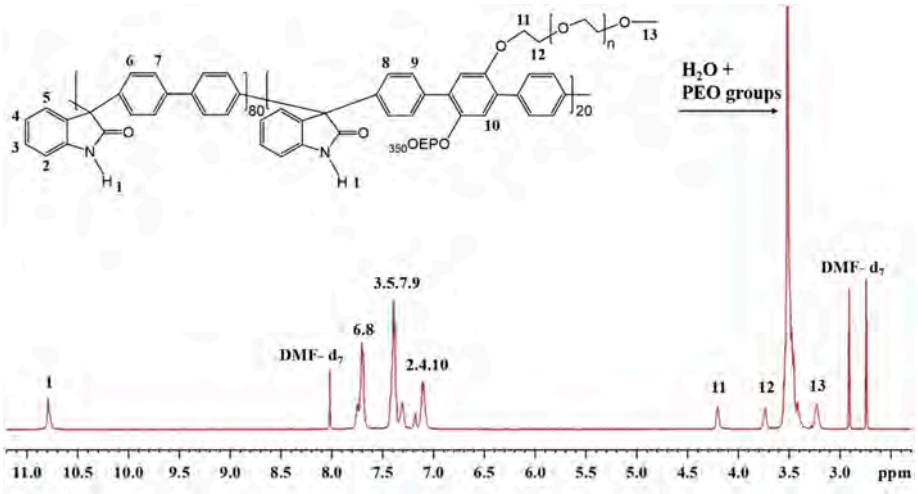

Fig. 2. ^{1}H NMR spectrum of P(IB-PEO)-20 copolymer in DMF-d_7.

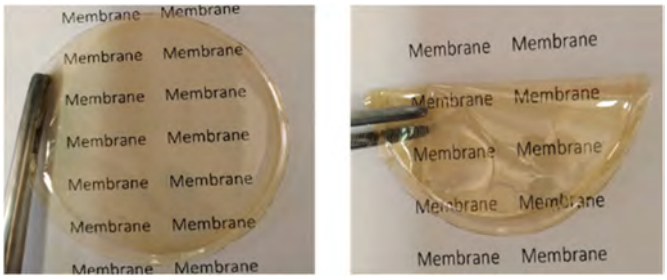

Fig. 3. Photographs of the prepared membranes based on P(IB-PEO)-20 copolymers indicating their transparency and flexibility.

were also reported for other PBI based blend membranes for use in electrochemical devices [45,46].

Regarding swelling (Fig. 4b), a moderate increase of the geometric surface area (SW_a) of the blend membranes was observed after doping varying between 9 and 16%, in contrast to thickness (SW_t), which is substantially increased up to 60%. However, the area and thickness increase observed in the blend membranes were significantly lower than that of pure *m*-PBI membrane (49% and 125%, respectively). The anisotropic swelling observed in these membranes was also reported for *m*-PBI membranes at KOH concentrations higher than about 10 wt% [24,25,47–49]. For PBI-based membranes, different swelling directions were observed for different molecular structures. In particular, Hu et al. reported that NPBI membrane doped in 6 M KOH showed a higher swelling thickness (120%) than area (~40%) [24]. On the contrary, the same group reported that the sulfonated analogue of NPBI exhibited much lower swelling thickness compared to area, probably due to nature of the polymer structure such as layered structure, intra-layer and interlayer molecular forces [25]. In our work, the high swelling thickness of blend membranes results from the increased polymer interchain distance of *m*-PBI backbones induced by the addition of KOH. Consequently, the prepared *m*-PBI rich blends display comparable electrolyte uptakes with pure *m*-PBI thus enabling the ionic conductivity while at the same time experience much lower swelling which is beneficial for the dimensional stability during electrolyser operation.

The contact angle of water for blends with 80, 70 and 60% *m*-PBI was measured to 84.3 ± 1.4°, 84.2 ± 1.2° and 82.9 ± 1.9° respectively (Fig. S5). The different membrane compositions do not display a clear trend within the error range, and contact angles show that in the dry state the membranes are not particularly hydrophilic. This indicates that the hydrophilic nature of the ion-solvating membranes is not realized until the doping with KOH.

3.2.2. Thermal stability

The TGA curves of the prepared blends are depicted in Fig. S6. All blend membranes exhibited an initial weight loss (13–14 wt%) up to 300 °C, ascribed to the residual water and DMA solvent that is held inside the matrix after drying under vacuum. Therefore, all curves were normalized based on the dry weight membrane to facilitate comparison. A small weight loss appeared at 350–500 °C and a second one at beyond 600 °C, corresponding to the thermal decomposition of P(IB-PEO)-20 copolymer and *m*-PBI backbone [47], respectively.

3.2.3. Mechanical properties

The mechanical robustness of pristine and KOH doped blend

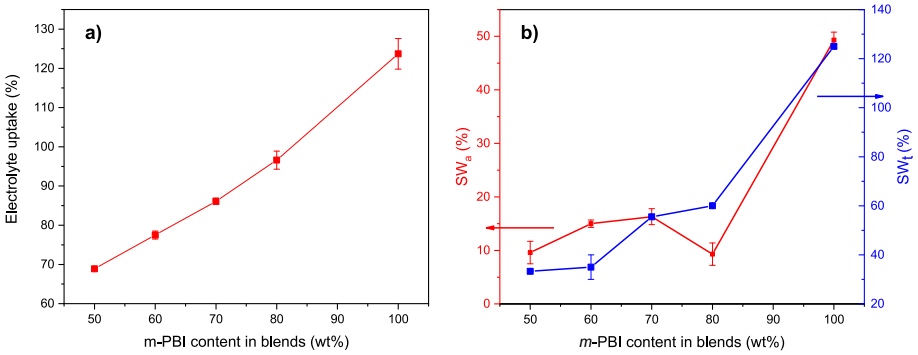

Fig. 4. a) Electrolyte uptake and b) area and thickness swelling plotted against *m*-PBI weight content after doping in 20 wt% KOH solution at 80 °C for 15 h.

membranes was assessed by measuring stress-strain curves. The tensile strength, the Young's Modulus and the stress-strain curves are given in Fig. 5a, b and 5c, 5d, respectively. Table 3 summarizes the mechanical properties of the blend membranes. Concerning the dry membranes, both blends showed similar tensile strength with that of pure *m*-PBI (159–167 MPa), while the Young's modulus of PBI80/P(IB-PEO) was slightly higher than that of the former (5212 and 4870 MPa for blend and pure *m*-PBI, respectively). The tensile strength of pristine *m*-PBI is predominately determined by the hydrogen bonding between imidazole moieties (–NH– and –N = groups) [47,48]. The incorporation of P(IB-PEO)-20 copolymer that contains N–H and carbonyl groups in the *m*-PBI matrix probably promotes the hydrogen bond formation between the two polymers, thus resulting in superior mechanical properties of the corresponding blends. After doping, both tensile strength and Young's modulus are drastically decreased due to water and KOH plasticization. These results are consistent with other PBI-based systems [24,25,47,48]. In particular, the KOH doped NPBI ion-solvating membrane presented reduced tensile strength compared to its dry analogue suggesting that KOH degraded the strength of the membrane which is probably ascribed to plasticization effect caused by water molecules [24]. In this work, the original hydrogen bonds between the two polymers are partially cleaved in the course of alkaline doping process, leading to increased polymer interchain distance of *m*-PBI backbones which is turn results in intermolecular forces decrease and eventually to mechanical strength deterioration. By increasing the weight content of P(IB-PEO)-20 copolymer in blends the mechanical properties are improved. Particularly, PBI70/P(IB-PEO) membrane shows a slightly increase in tensile strength (20 MPa) and a significant improvement in elastic modulus (131%) compared to that of PBI80/P(IB-PEO).

Table 3
Summary of mechanical properties of pristine blend and alkali doped blend membranes.

Membrane type	Tensile strength (MPa)	Elongation at break (%)	Young's Modulus (MPa)
Dry membranes			
m-PBI	160 ± 40	4 ± 1	4870 ± 785
PBI80/P(IB-PEO)	159 ± 25	4 ± 1	5212 ± 881
PBI70/P(IB-PEO)	167 ± 9	7 ± 2	4869 ± 235
20 wt% KOH doped membranes			
m-PBI	19 ± 7	101 ± 53	136 ± 45
PBI80/P(IB-PEO)	14 ± 5	48 ± 19	134 ± 73
PBI70/P(IB-PEO)	20 ± 2	79 ± 18	310 ± 35
After alkaline treatment for 30 days			
PBI80/P(IB-PEO)	17 ± 4	41 ± 20	327 ± 24

3.2.4. *Ionic conductivity*

The conductivity of all prepared membranes was studied at room temperature, but due to the low ionic conductivity of the blend membranes with 50 and 60 wt% *m*-PBI content (not shown here), only the blend membranes with 70 and 80 wt% *m*-PBI content were further evaluated. Thus, the ion conductivity of the latter was studied as a function of temperature (Fig. 6a). The conductivity was found to increase with increasing temperature, as expected owing to the increased electrolyte absorption and ion mobility. The conductivity values for PBI80/P(IB-PEO) and PBI70/P(IB-PEO) at 80 °C was 110 mS cm^{-1} and 74 mS cm^{-1}, respectively. The higher ion conductivity of the former can be probably attributed to its higher electrolyte uptake. For comparison, the conductivity of pure PBI in 20 wt% KOH is 85, 102, 107 and 110 mS cm^{-1} at 20, 40, 60 and 80 °C [18]. Both blend membranes showed high conductivity values, confirming their potential for use in electrolyser systems. Fig. 6b presents the Arrhenius plots for the two blend membranes. The activation energy (E_a) for the two blend membranes was in the range from 14 to 19 kJ/mol. For comparison, the activation energy of the KOH doped *m*-PBI was found to be in the range of 8–16 kJ/mol and tended to increase slightly with increasing KOH concentration [18]. The activation energy values of both systems fall in the range for the

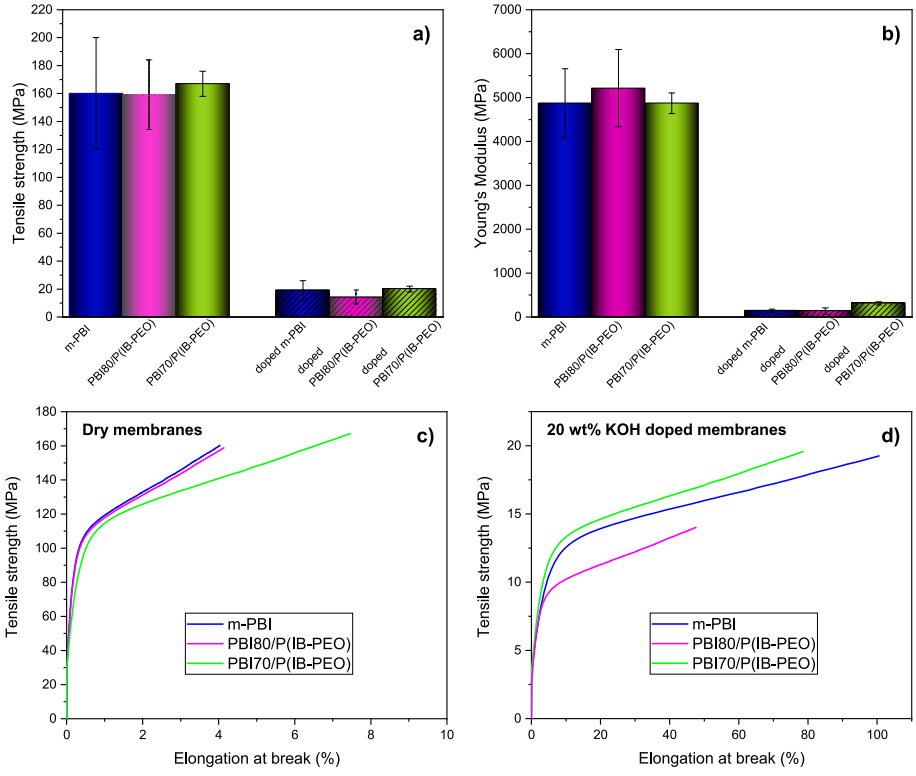

Fig. 5. a) Tensile strength, b) Young's Modulus and c), d) Stress-strain curves of the dry and KOH doped blend membranes in 20 wt% KOH at 80 °C for 15 h.

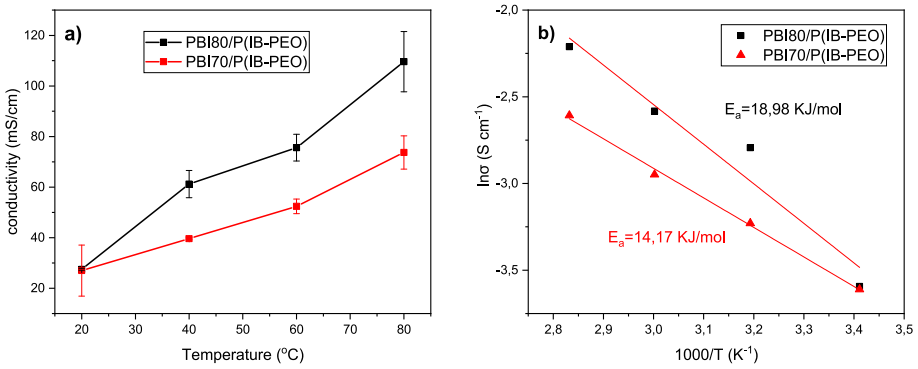

Fig. 6. a) Ionic conductivity as a function of temperature and b) Arrhenius plots of blend membranes.

Grotthuss transportation mechanism.

3.2.5. *Alkaline stability*

The alkaline stability of membranes is considered a critical factor that strongly affects the durability of alkaline water electrolyzers. The alkaline stability was assessed by immersing the membranes in 20 wt% KOH solution at 80 °C. After 1 month, none of the membranes (80/20, 70/30 and 60/40 compositions) were broken and they all preserved their mechanical robustness as illustrated in Fig. S7. In addition, PBI80/P(IB-PEO) membrane shows even a slight increase in tensile strength while the Young's modulus is increased by 144% compared to the corresponding blend before aging (Table 3). One possible explanation is that *m*-PBI's imidazolide groups strongly interact with isatin and/or PEO groups via ion-dipole interactions, contributing also to the mechanical strength. Fig. 7 shows the room temperature ion conductivity of the blends PBI80/P(IB-PEO) and PBI70/P(IB-PEO) as a function of the aging time. The conductivity of both membranes remained almost unchanged after 1 month in hot alkaline solution at 80 °C, (retain 96–98% of their origin conductivity), indicating their excellent hot alkaline resistance. It should be stressed out that during the aging test the conductivity values were slightly scattered probably owing to the variation of samples' thickness, which affects electrolyte uptake.

Further, a comparison of the ATR-FT-IR data did not indicate degradation (Fig. 8) since no new peaks which would suggest hydrolysis of imidazole ring or hydroxide attack to carbonyl group of isatin were observed. In addition, the TGA study reveals that aging did not affect the thermo-oxidative stability of the blends, particularly blend PBI80/P(IB-PEO) exhibits even improved thermal stability compared to the non-treated analogue, as depicted in Fig. S6.

The excellent alkaline stability could possibly be attributed to the strong attractive interactions (hydrogen bonding, ion-dipole) developed between the two polymers. It is worth to mention that although deprotonation of N–H group of isatin can take place under alkaline conditions leading to the formation of azanion [50], the presence of water promotes the reversible reaction. In addition, despite being vulnerable to hydroxide attack, C2- carbonyl group of isatin was not degraded via ring-opening. The excellent alkaline resistance is possibly related to the presence of adjacent phenyl ring to C2-carbon, thereby increasing the sterical hindrance and stabilization against hydroxide attack at this carbon. However, even if ring opening occurs, this degradation pathway cannot lead to polymer backbone cleavage as reported by Long et al. [51], highlighting the excellent alkaline stability of isatin based copolymers. The alkaline stability is further supported by the participation of isatin group in hydrogen bonding/columbic interactions with K^+. After aging, the peak at 1702 cm^{-1} attributed to the *ν* (C═O) stretching vibration of isatin becomes broader while a new peak appears at 1689 cm^{-1} indicating that carbonyl group probably participates in hydrogen bond formation or ionic interaction with K^+ (Fig. S8) [50]. In addition, the band at 1610 cm^{-1} corresponding to *ν* (C═N) bond of *m*-PBI is significantly reduced and is shifted towards lower

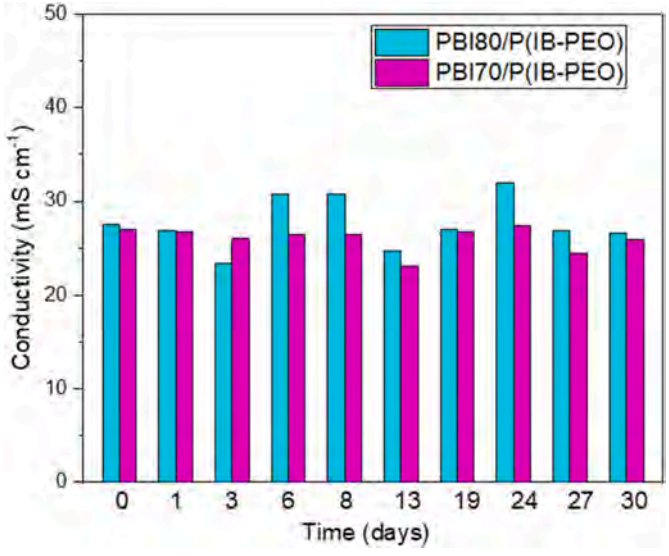

Fig. 7. Ionic conductivity of the blend membranes after aging in 20 wt% aqueous KOH solution at 80 °C (measured at room temperature in 20 wt % KOH).

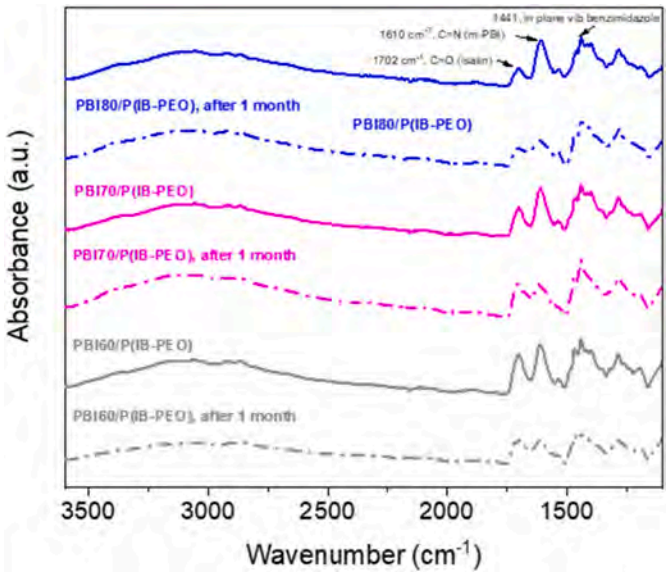

Fig. 8. ATR-FT-IR spectra of blend membranes before and after aging in 20 wt % KOH solution for 30 days at 80 °C.

wavenumbers (1593 cm^{-1}), suggesting the hydrogen bond formation.

3.2.6. Electrolysis cell testing

For single cell electrolysis testing, the PBI80/P(IB-PEO) composition was down selected, since it displayed the best overall characteristics. The membrane was cast to a dry thickness of ca 100 μm, and was approximately 150 μm after doping, just prior to mounting. Polarization curves recorded at different temperatures are shown in Fig. 9. The overall cell performance is limited by the choice of plain nickel foam electrodes, but they serve as a stable choice for benchmarking membranes, as they are not dependent on optimized catalyst layers and ionomers to provide reliable measurements. The slope at high current density is often associated with ohmic losses, which predominantly relate to the membrane resistance in idealized systems. However, as evident from the figure, the cell does not inhibit a fully linear trend even at high current density.

To quantify the data, linear fits were done for data points at 300 mA cm^{-2} and above. The data is summarized in Table 4, together with extracted R_s values from impedance fitting. The membrane resistance, R_s, from impedance data was obtained by fitting an L-R-RQ-RQ-RQ equivalent circuit model. Nyquist plots and associated fits are available in the supplementary, in Fig. S9. Two of the RQ elements represent the kinetic parts of the anode and cathode respectively, while the third RQ element is ascribed to the porous nature of the electrodes and is largely current density independent. However, more detailed analysis of the EIS response is beyond the scope of this work, where emphasis is on the membrane, and the obtained resistance values. The data in Table 4 is from data recorded at 10 mA cm^{-2}, both at beginning (BoT) and end of test (EoT). It is clear that values obtained by linear fits are not representative for the membrane performance, as it shows significantly higher resistance values, and as such the slope does not represent a good method for assessing membrane resistance with the used electrode configuration.

Comparing the obtained data with *ex-situ* conductivity data, we observe somewhat lower conductivities *in-situ*. This could be ascribed to differences in conductivity due to contributions from K^+ under non-polarized conditions *ex-situ*, or be influenced by the presence of bubbles in the electrode-membrane interface under direct current conditions even at low current density. Alternatively, it may be influenced in part by the local electrolyte environment in the cell, such as

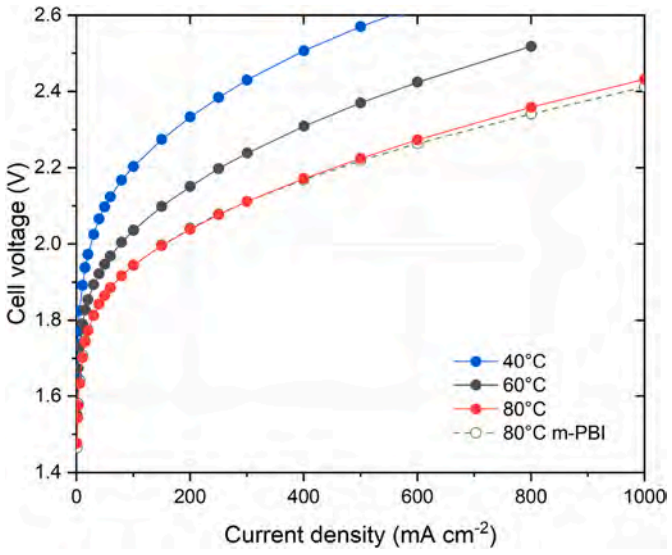

Fig. 9. Polarization curves recorded at 40, 60 and 80 °C in 20 wt% KOH, using a 150 μm PBI80/P(IB-PEO) membrane, with Ni foam electrodes. Polarization curves of a commercial 100 μm m-PBI in 25 wt% at 80 °C is shown for reference.

Table 4
Membrane resistance obtained from linear fits and impedance data. Calculated conductivity is based on a membrane thickness of 150 μm.

Temperature	Linear fit	10 mA cm^{-2}, BoT		10 mA cm^{-2}, EoT	
	R	R_s	σ	R_s	σ
°C	Ω cm^2	Ω cm^2	S cm^{-1}	Ω cm^2	S cm^{-1}
40	0.662	0.349	0.043	0.304	0.049
60	0.565	0.302	0.050	0.258	0.058
80	0.454	0.255	0.059	0.215	0.069

concentration gradients, which build up during electrolyzer operation. Another observation is the apparent decrease in resistance over the course of the four day test. Unlike AEM's, there are no ion exchange groups in ion-solvating membranes that can degrade, and thereby cause a direct loss of conductivity [16]. One possible explanation is an increased doping degree as the membrane is exposed to KOH at higher temperatures in the cell test. Prior to the cell testing, the membrane is doped only at room temperature, but the electrolyte uptake is higher at 80 °C than at lower temperatures (Table S1). Another possibility is slight changes in concentration and concentration gradients across the cell resulting in a slightly different environment for the membrane between beginning and end of test. Such changes can facilitate morphological rearrangements and allow the membrane to take up more electrolyte and thereby decrease the cell resistance. For pure *m*-PBI, the morphological makeup of the membrane has recently been shown to have drastic influence on the membrane conductivity [52]. While it was previously shown that the electrolyte uptake and structural rearrangements of pure *m*-PBI occur on the minutes to hours' time scale [53], the blend nature of this material may exhibit a different and more constrained behaviour. It can be envisioned that the higher mobility at increased temperature can promote further restructuring of the polymers in the membrane allowing for extra electrolyte uptake. Alternatively, membrane backbone degradation could manifest as gradual thinning, which due to the presence of electrolyte would not negatively influence cell resistance, but rather increase the KOH fraction between the electrodes and thus reducing cell resistance. Nonetheless, the membrane looked pristine after test, as shown in Fig. S10, with no indication of any substantial damage during the experiment.

3.2.7. Hydrogen crossover

The hydrogen crossover across the membrane is a severely neglected issue in literature, even though separation of gas is a critical membrane function. Diffusive crossover has been shown to be quite substantial for PEM systems [54], but it is not well investigated for alkaline membranes. It has previously been shown by Trinke et al. that crossover measured under cell conditions, does not necessarily represent one well determined material parameter [55]. Rather, it is a combined result of membrane and electrode configuration, due to the highly oversaturated nature of the gas evolved at the electrodes. In this work, we have examined the hydrogen crossover as part of the electrolysis test by applying steady state conditions for 6 h steps and measuring the resulting hydrogen in oxygen levels. Fig. 10a shows the hydrogen in oxygen level, corrected for the applied nitrogen carrier gas, whereas Fig. 10b shows the calculated hydrogen flux density. Equivalent data for the direct measurement influenced by the nitrogen is shown in Fig. S11, and the underlying time dependent data can be seen in Fig. S12 for each temperature sequence. Measurements exhibit a steep rise or drop a few minutes after changing current setpoint, after which a new level set in, with some variation over time due to fluctuations in the balance of plant in our test setup. Note that the variations generally are in the timescale of 10–30 min. The data plotted in Fig. 10 represent average values over the last 5 h of each setpoint.

Assuming constant diffusive flux on basis of the hydrogen partial pressure on each side of the membrane, one will expect a constant flux, and downward trending hydrogen levels as current density goes up. This

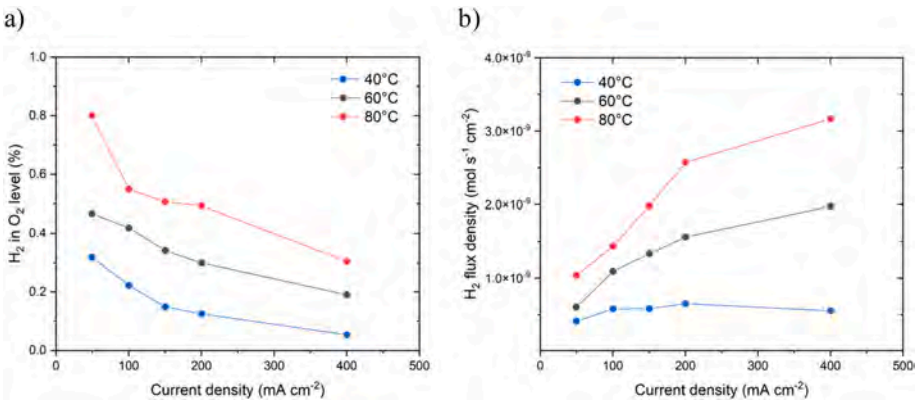

Fig. 10. Crossover measurements of a) nitrogen corrected hydrogen in oxygen level and b) corresponding hydrogen flux density values.

is generally observed in this current range, for both other ion-solvating membranes [52], diaphragms [55,56], as well as PEM systems [55,57]. At a first glance we observe the expected drop in hydrogen level with current density, as the degree of dilution by the generated oxygen increase. However, investigating the corresponding crossover flux, we see a general increasing trend with current density, which we ascribe to a higher degree of local supersaturation at the electrode-membrane interface, causing a stronger local concentration gradient of dissolved hydrogen across the membrane. Similar observations have been observed for both PEM systems and alkaline separators, and the apparent non-linear behaviour of the current density dependent increase in hydrogen flux resemble data previously reported for Zirfon with a similar electrode configuration [55,56]. It should also be remarked that the direction of the electroosmotic drag in alkaline environment is from the cathode towards the anode, which should contribute to increasing flux of H_2 with increasing current density. On the other hand, at high current densities a larger KOH concentration gradient is established across the membrane, and common osmotic pressure will tend to drive the electrolyte towards the cathode side, resulting in dryout and cell failure if electrolyte circulation is completely separated. Previous work estimates crossover contributions due to electroosmotic drag to be negligible compared to diffusion [55,58], but recent work suggests that the effect can become significant at high current densities [57]. The measurements here were recorded in a partially separated electrolyte configuration, in which the electrolyte loops are connected via a by-pass tube, located between outlet of the gas-separator vessels and the circulation pumps. This allows for electrolyte level equilibration between the primary KOH storage vessels, as we otherwise observe severe electrolyte migration from anode to cathode. This causes drastically increased crossover as the anolyte loop eventually dry out and ultimately cell failure. The influence on measured levels using partially separated electrolyte loops has previously been shown to be negligible when using Zirfon [59]. While we also expect the effect to be minor in our case, it is not impossible that dissolved hydrogen in the electrolyte by-pass migrating towards the anode can contribute to some degree. Different measurements carried out with a closed by-pass displayed a severe accumulation of electrolyte on the cathode side, and we expect a counteracting movement of electrolyte in the by-pass channel. The observed behaviour also show a very strong increase with temperature. The effect is much more pronounced than observed with Zirfon [59]. While solubility decrease with temperature, that effect is likely inhibited as the local conditions are supersaturated. As such, temperature increases the diffusivity, and perhaps influences the morphology of the membrane, ultimately leading to a substantial increase in crossover flux. Comparing the crossover level at 40 °C and 100 mA cm^{-2} between the first day to the last day of testing, the hydrogen in oxygen level increase from ca 0.22% to about 0.29%, suggesting some morphological changes of the membrane across the duration of the experiment. Assessing specific permeability values is tricky from the obtained data due to the supersaturated nature of the electrolyte. By linear extrapolation of the 50–200 mA cm^{-2} datapoints to zero current density, we calculate specific permeabilities of 5.6, 5.6 and 7.1 × 10^{-12} mol s^{-1} cm^{-1} for 40, 60 and 80 °C respectively. This is very similar to values observed for Tokuyama A201 by Ito et al. [60], although the detailed conditions and cell configuration vary. However, clearly the almost identical calculated specific permeabilities does not adequately catch the temperature and current density dependent behaviour in our case, which as an example shows more than 5 times higher H_2 in O_2 levels at 400 mA cm^{-2} going from 40 to 80 °C.

4. Conclusions

Alkaline stable monomers and their corresponding copolymers containing both PEO and isatin segments with ion-solvating properties were synthesized via super acid catalyzed hydroxyalkylation. The synthesized copolymers show excellent film forming ability, high thermal stability, moderate KOH uptake and conductivity. To boost electrolyte absorption and consequently conductivity, these copolymers were blended with polybenzimidazole at different weight ratios. The fabricated membranes exhibit a moderate swelling ability compared to that of neat *m*-PBI and high electrolyte uptakes (up to 97 wt%). The PBI80/P(IB-PEO) blend showed the highest ionic conductivity value of 110 mS cm^{-1} at 80 °C. Evaluation of the mechanical properties revealed that the KOH doped PBI70/P(IB-PEO) membrane possesses a tensile strength of 20 MPa and a much higher Young's modulus (131%) compared to that of PBI80/P(IB-PEO). Alkaline stability study unveiled the excellent alkaline resistance of the prepared PBI80/P(IB-PEO) and PBI70/P(IB-PEO) membranes since they preserved 96–98% of their original conductivity after aging for 1 month in 20 wt% KOH solution at 80 °C. Further, the changes in the mechanical properties were also recorded after aging revealing that the aged PBI80/P(IB-PEO) membrane exhibits superior Young's modulus (144% increase) compared to that of the non-aged analogue, probably attributed to the strong interactions developed between *m*-PBI's imidazolide groups with isatin and/or PEO groups. Single cell electrolyzer testing of the selected PBI80/P(IB-PEO) membrane demonstrated that *in situ* calculated values are lower than *ex-situ* conductivity values. In addition, hydrogen crossover was measured and hydrogen in oxygen levels were found comparable to similar work in literature, showing estimated specific permeabilities around 5 × 10^{-12} mol s^{-1} cm^{-1}.

Author Statement

Maria Makrygianni: Investigation, Writing-original draft, **Stefania Aivali:** Investigation, **Yifan Xia:** Investigation, **Mikkel R. Kraglund**: Investigation, Writing-original draft, Writing-review & editing, **David**

Aili: Methodology, Resources, Supervision, Visualization, Writing-original draft, review & editing, **Valadoula Deimede**: Conceptualization, Visualization, Methodology, Resources, Writing-original draft, Writing-review & editing, Supervision.

Declaration of competing interest

The authors declare that they have no known competing financial interests or personal relationships that could have appeared to influence the work reported in this paper.

Data availability

The authors are unable or have chosen not to specify which data has been used.

Acknowledgements

This work was funded by the European Union Horizon H2020 project "Materials for next generation of alkaline electrolyzer (NEXTAEC), grant agreement No: 862509.

Appendix A. Supplementary data

Supplementary data to this article can be found online at https://doi.org/10.1016/j.memsci.2022.121331.

References

[1] B. Pivovar, N. Rustagi, S. Satyapal, Hydrogen at scale (H_2@Scale): key to a clean, economic, and sustainable energy system, Electrochem. Soc. Interface 27 (2018) 47–52.
[2] P.E. Dodds, I. Staffell, A.D. Hawkes, F. Li, P. Grunewald, W. McDowall, P. Ekins, Hydrogen and fuel cell technologies for heating: a review, Int. J. Hydrogen Energy 40 (2015) 2065–2083.
[3] J. Tollefson, Hydrogen vehicles: fuel of the future? Nature 464 (2010) 1262–1264.
[4] T.A. Napp, A. Gambhir, T.P. Hills, N. Florin, P.S. Fennell, A review of the technologies, economics and policy instruments for energy-intensive manufacturing industries, Renew. Sustain. Energy Rev. 30 (2014) 616–640.
[5] I. Staffell, D. Scamman, A. Velazquez Abad, P. Balcombe, P.E. Dodds, P. Ekins, N. Shah, K.R. Ward, The role of hydrogen and fuel cells in the global energy system, Energy Environ. Sci. 12 (2019) 463–491.
[6] J.A. Turner, Sustainable hydrogen production, Science 305 (2017) 972–974.
[7] D. Li, A.R. Motz, C. Bae, C. Fujimoto, G. Yang, F.-Y. Zhang, K.E. Ayers, Y.S. Kim, Durability of anion exchange membrane water electrolyzers, Energy Environ. Sci. 14 (2021) 3393–3419.
[8] H.A. Miller, K. Bouzek, J. Hnat, S. Loos, C. Immanuel Bernäcker, T. Weißgärber, L. Röntzschc, J. Meier-Haack, Green hydrogen from anion exchange membrane water electrolysis: a review of recent developments in critical materials and operating conditions, Sustain. Energy Fuels 4 (2020) 2114–2133.
[9] J.R. Varcoe, P. Atanassov, D.R. Dekel, A.M. Herring, M.A. Hickner, P.A. Kohl, A. R. Kucernak, W.E. Mustain, K. Nijmeijer, K. Scott, T. Xu, L. Zhuang, Anion-exchange membranes in electrochemical energy systems, Energy Environ. Sci. 7 (2014) 3135–3191.
[10] H. Li, N. Yu, F. Gellrich, A.K. Reumert, M.R. Kraglund, J. Dong, D. Aili, J. Yang, Diamine crosslinked anion exchange membranes based on poly(vinyl benzyl methylpyrrolidinium) for alkaline water electrolysis, J. Membr. Sci. 633 (2021), 119418.
[11] H. Li, M.R. Kraglund, A.K. Reumert, X. Ren, D. Aili, J. Yang, Poly(vinyl benzyl methylpyrrolidinium) hydroxide derived anion exchange membranes for water electrolysis, J. Mater. Chem. 7 (2019) 17914–17922.
[12] X. Chu, Y. Shi, L. Liu, Y. Huang, N. Li, Piperidinium-functionalized Anion Exchange Membranes and its application in alkaline fuel cells and water electrolysis, J. Mater. Chem. 7 (2019) 7717–7727.
[13] H.J. Park, S.Y. Lee, T.K. Lee, H.-J. Kim, Y.M. Lee, N3-butyl imidazolium-based anion exchange membranes blended with poly(vinyl alcohol) for alkaline water electrolysis, J. Membr. Sci. 611 (2020), 118355.
[14] C.G. Arges, L. Zhang, Anion exchange membranes evolution towards high hydroxide ion conductivity and alkaline resiliency, ACS Appl. Energy Mater. 1 (2018) 2991–3012.
[15] W. You, K.J.T. Noonan, G.W. Coates, Alkaline-stable anion exchange membranes: a review of synthetic approaches, Prog. Polym. Sci. 100 (2020), 101177.
[16] M.R. Kraglund, M. Carmo, G. Schiller, S.A. Ansar, D. Aili, E. Christensen, J. O. Jensen, Ion solvating membranes as a new approach towards high rate alkaline elecrolyzers, Energy Environ. Sci. 12 (2019) 3313–3318.
[17] D. Aili, A.G. Wright, M.R. Kraglund, K. Jankova, S. Holdcroft, J.O. Jensen, Towards a stable ion-solvating polymer electrolyte for advanced alkaline water electrolysis, J. Mater. Chem. 5 (2017) 5055–5066.
[18] M.R. Kraglund, D. Aili, A.K. Jankova, E. Christensen, Q. Li, J.O. Jensen, Zero-gap alkaline water electrolysis using ion-solvating polymer electrolyte membranes at reduced KOH concentrations, J. Electrochem. Soc. 163 (2016) F3125–F3131.
[19] S. Guinot, E. Salmon, J.F. Penneau, J.F. Fauvarque, A new class of PEO-based SPEs: structure, conductivity and application to alkaline secondary batteries, Electrochim. Acta 43 (1998) 1163–1170.
[20] I. Palacios, R. Castillo, R.A. Vargas, Thermal and transport properties of the polymer electrolyte based on poly(vinyl alcohol)–KOH–H2O, Electrochim. Acta 48 (2003) 2195–2199.
[21] A. Lewandowski, K. Skorupska, J. Malinska, Novel poly(vinyl alcohol)–KOH–H_2O alkaline polymer electrolyte, Solid State Ionics 133 (2000) 265–271.
[22] B. Xing, O. Savadogo, Hydrogen/oxygen polymer electrolyte membrane fuel cells (PEMFCs) based on alkaline-doped polybenzimidazole (PBI) Electrochem, Commun. Now. 2 (2000) 697–702.
[23] G. Merle, M. Wessling, K. Nijmeijer, Anion-exchange membranes for alkaline fuel cells: a review, J. Membr. Sci. 377 (2011) 1–35.
[24] X. Hu, M. Liu, Y. Huang, L. Liu, N. Li, Sulfonate-functionalized polybenzimidazole as ion-solvating membrane toward high-performance alkaline water electrolysis, J. Membr. Sci. 663 (2022), 121005.
[25] B. Hu, Y. Huang, L. Liu, X. Hu, K. Geng, Q. Ju, M. Liu, J. Bi, S. Luo, N. Li, A stable ion-solvating PBI electrolyte enabled by sterically bulky naphthalene for alkaline water electrolysis, J. Membr. Sci. 643 (2022), 120042.
[26] A.D. Mohanty, S.E. Tignor, J.A. Krause, Y.K. Choe, C. Bae, Systematic alkaline stability study of polymer backbones for anion exchange membrane applications, Macromolecules 49 (2016) 3361–3372.
[27] E.J. Park, Y.S. Kim, Quaternized aryl ether-free polyaromatics for alkaline membrane fuel cells: synthesis, properties, and performance – a topical review, J. Mater. Chem. 6 (2018) 15456–15477.
[28] A.M. Diaz, M.G. Zolotukhin, S. Fomine, R. Salcedo, O. Manero, G. Cedillo, V. M. Velasco, M.T. Guzman, D. Fritsch, A.F. Khalizov, A novel, one-pot synthesis of 3F, 5F and 8F aromatic polymers, Macromol. Rapid Commun. 28 (2007) 183–187.
[29] A.R. Cruz, M.C.G. Hernandez, M.T. Guzmán-Gutiérrez, M.G. Zolotukhin, S. Fomine, S.L. Morales, H. Kricheldorf, E.S. Wilks, J. Cárdenas, M. Salmón, Precision synthesis of narrow polydispersity, ultrahigh molecular weight linear aromatic polymers by A 2 + B 2 nonstoichiometric step- selective polymerization, Macromolecules 45 (2012) 6774–6780.
[30] L.I. Olvera, M.T. Guzmán-Gutiérrez, M.G. Zolotukhin, S. Fomine, J. Cárdenas, F. A. Ruiz-Trevino, D. Villers, T.A. Ezquerra, E. Prokhorov, Novel high molecular weight aromatic fluorinated polymers from one-pot, metal-free step polymerizations, Macromolecules 46 (2013) 7245–7256.
[31] J. Wang, Y. Zhao, B.P. Setzler, S. Rojas-Carbonell, C. Ben Yehuda, A. Amel, M. Page, L. Wang, K. Hu, L. Shi, S. Gottesfeld, B. Xu, Y. Yan, Poly(aryl piperidinium) membranes and ionomers for hydroxide exchange membrane fuel cells, Nat. Energy 4 (2019) 392–398.
[32] J.S. Olsson, T.H. Pham, P. Jannasch, Poly(arylene piperidinium) hydroxide ion exchange membranes : synthesis, alkaline stability, and conductivity, Adv. Funct. Mater. 28 (2018), 1702758.
[33] X. Hu, Y. Huang, L. Liu, Q. Ju, X. Zhou, X. Qiao, Z. Zheng, N. Li, Piperidinium functionalized aryl-ether free polyaromatics as anion exchange membrane for water electrolysers: performance and durability, J. Membr. Sci. 621 (2021), 118964.
[34] W.H. Lee, Y.S. Kim, C. Bae, Robust hydroxide ion conducting poly(biphenyl alkylene)s for alkaline fuel cell membranes, ACS Macro Lett. 4 (2015) 814–818.
[35] B. Xue, W. Cui, S. Zhou, Q. Zhang, J. Zheng, S. Li, S. Zhang, Facile preparation of highly alkaline stable poly(arylene−imidazolium) anion exchange membranes through an ionized monomer strategy, Macromolecules 54 (2021) 2202–2212.
[36] S. Zhang, X. Zhua, C. Jin, Development of high-performance anion exchange membrane fuel cell using poly(isatin biphenylene) with flexible heterocycle quaternary ammonium cations, J. Mater. Chem. 7 (2019) 6883–6893.
[37] T.H. Pham, J.S. Olsson, P. Jannasch, Effects of the N-alicyclic cation and backbone structures on the performance of poly(terphenyl)-based hydroxide exchange membranes, J. Mater. Chem. 7 (2019) 15895–15906.
[38] N. Chen, C. Hu, H.H. Wang, S.P. Kim, H.M. Kim, W.H. Lee, J.Y. Bae, J.H. Park, Y. M. Lee, Poly(alkyl-terphenyl piperidinium) ionomers and membranes with outstanding alkaline membrane fuel cell performance of 2.58 W cm^{-2}, Angew. Chem., Int. Ed. Engl. 60 (2021) 7710–7718.
[39] R. Ren, S. Zhang, H.A. Miller, F. Vizza, J.R. Varcoe, Q. He, Facile preparation of an ether-free anion exchange membrane with pendant cyclic quaternary ammonium groups, ACS Appl. Energy Mater. 2 (2019) 4576–4581.
[40] R. Ren, S. Zhang, H.A. Miller, F. Vizza, J.R. Vacroe, Q. He, Facile preparation of novel cardo poly(oxindolebiphenylene) with pendent quaternary ammonium by super-acid catalyzed polyhydroxyalkylation for anion exchange membranes, J. Membr. Sci. 591 (2019), 117320.
[41] D. Aili, M.K. Hansen, R.F. Renzaho, Q. Li, E. Christensen, J.O. Jensen, N.J. Bjerrum, Heterogeneous anion conducting membranes based on linear and cross-linked KOH doped polybenzimidazole for alkaline water electrolysis, J. Membr. Sci. 447 (2013) 424–432.
[42] A. Vöge, V. Deimede, F. Paloukis, S.G. Neophytides, J.K. Kallitsis, Synthesis and properties of aromatic polyethers containing poly(ethylene oxide) side chains as polymer electrolytes for lithium ion batteries, Mater. Chem. Phys. 148 (2014) 57–66.
[43] A. Ioannidi, D. Vroulias, J. Kallitsis, T. Ioannides, V. Deimede, Synthesis and characterization of poly (ethylene oxide) based copolymer membranes for efficient

gas/vapor separation: effect of PEO content and chain length, J. Membr. Sci. 632 (2021), 119353.
[44] M.T. Guzmán-Gutiérrez, D.R. Nieto, S. Fomine, S.L. Morales, M.G. Zolotukhin, C. G. Hernandez, H. Kricheldorf, E.S. Wilks, Dramatic enhancement of superacid-catalyzed polyhydroxyalkylation reactions, Macromolecules 44 (2011) 194–202.
[45] A. Konovalova, H. Kim, S. Kim, A. Lim, H.S. Park, M.R. Kraglund, D. Aili, J.H. Jang, H.-J. Kim, D. Henkensmeier, Blend membranes of polybenzimidazole and an anion exchange ionomer (FAA3) for alkaline water electrolysis: improved alkaline stability and conductivity, J. Membr. Sci. 564 (2018) 653–662.
[46] D. Herranz, R. Escudero-Cid, M. Montiel, C. Palacio, E. Fatás, P. Ocón, Poly(vinyl alcohol) and poly(benzimidazole) blend membranes for high performance alkaline direct ethanol fuel cells, Renew. Energy 127 (2018) 883–895.
[47] D. Aili, K. Jankova, J. Han, N.J. Bjerrum, J.O. Jensen, Q. Li, Understanding ternary poly(potassium benzimidazolide)-based polymer electrolytes, Polymer 84 (2016) 304–310.
[48] L. Zheng, T.S. Zhao, L. An, G. Zhao, X.H. Yan, Physicochemical properties of alkaline doped polybezimidazole membranes for anion exchange membrane fuel cells, J. Membr. Sci. 493 (2015) 340–348.
[49] R.N. Couto, J.J. Linares, KOH-doped polybenzimidazole for alkaline direct glycerol fuel cells, J. Membr. Sci. 486 (2015) 239–247.
[50] P. Tisovský, R. Šandrik, M. Horváth, J. Donovalová, J. Filo, M. Gáplovský, K. Jakusová, M. Cigáň, R. Sokolík, A. Gáplovský, Effect of structure on charge distribution in the isatin anions in aprotic environment: spectral study, Molecules 22 (2017) 1961.
[51] C. Long, T. Zhao, L. Tian, Q. Liu, F. Wang, Z. Wang, H. Zhu, Highly stable and conductive multicationic poly(biphenyl indole) with extender side chains for anion exchange membrane fuel cells, ACS Appl. Energy Mater. 4 (2021) 6154–6165.
[52] M.L.A. Trisno, A. Dayan, S.J. Lee, F. Egert, M. Gerle, M.R. Kraglund, J.O. Jensen, D. Aili, A. Roznowska, A. Michalak, H.S. Park, F. Razmjooei, S.-A. Ansar, D. Henkensmeier, Reinforced gel-state polybenzimidazole hydrogen separators for alkaline water electrolysis, Energy Environ. Sci. 15 (2022) 4362–4375.
[53] E. Babcocka, N. Szekelya, A. Konovalova, Y. Lind, M.-S. Appavou, G. Mangiapia, Z. Revay, C. Stieghorst, O. Holderer, D. Henkensmeier, W. Lehnert, M. Carmo, Using neutron methods SANS and PGAA to study evolution of structure and composition of alkali-doped polybenzimidazole membranes, J. Membr. Sci. 577 (2019) 12–19.
[54] U. Babic, M. Suermann, F.N. Buchi, L. Gubler, T.J. Schmidt, Review—identifying critical gaps for polymer electrolyte water electrolysis development, J. Electrochem. Soc. 164 (2017) F387–F399.
[55] P. Trinke, P. Haug, J. Brauns, B. Bensmann, R. Hanke-Rauschenbach, T. Turek, Hydrogen crossover in PEM and alkaline water electrolysis: mechanism, direct comparison and mitigation strategies, J. Electrochem. Soc. 165 (2018) F502–F513.
[56] J. Brauns, J. Schönebeck, M.R. Kraglund, D. Aili, J. Hnát, J. Žitka, W. Mues, J. O. Jensen, K. Bouzek, T. Turek, Evaluation of diaphragms and membranes as separators for alkaline water electrolysis, J. Electrochem. Soc. 168 (2021), 014510.
[57] A. Martin, P. Trinke, B. Bensmann, R.H. Rauschenbach, Hydrogen crossover in PEM water electrolysis at current densities up to 10 A cm^{-2}, J. Electrochem. Soc. 169 (2022), 094507.
[58] M. Schalenbach, M. Carmo, D.L. Fritz, J. Mergel, D. Stolten, Pressurized PEM water electrolysis: efficiency and gas crossover, Int. J. Hydrogen Energy 38 (2013) 14921–14933.
[59] P. Haug, M. Koj, T. Turek, Influence of process conditions on gas purity in alkaline water electrolysis, Int. J. Hydrogen Energy 42 (2017) 9406–9418.
[60] H. Ito, N. Kawaguchi, S. Someya, T. Munakata, Pressurized operation of anion exchange membrane water electrolysis, Electrochim. Acta 297 (2019) 188–196.